THE ASTROPHYSICAL JOURNAL, 397:542–551, 1992 October 1

IRAS[1] OBSERVATIONS AND THE STELLAR CONTENT OF H II REGIONS IN THE LARGE MAGELLANIC CLOUD

KATHLEEN DEGIOIA-EASTWOOD
Department of Physics and Astronomy, Northern Arizona University, Box 6010, Flagstaff, AZ 86011
Received 1991 June 10; accepted 1992 April 9

ABSTRACT

IRAS far-infrared fluxes are presented for six H II regions in the Large Magellanic Cloud. These regions are the sites of recent, massive star formation where the radiative heating source is young stars rather than the general interstellar radiation field. As such, the observations become building blocks for the interpretation of far-infrared emission from spatially unresolved galaxies. In addition, the multiwavelength luminosities of the region then probe the young stellar upper initial mass function. With the long-range goal of determining the stellar content of unresolved star-forming regions, we present the results of a simple model which combines the infrared data with existing Hα/Hβ and thermal radio data. For the two OB associations where the mass function has been determined directly, the model correctly "predicts" a solar neighborhood upper mass function within the uncertainties. No evidence is found for upper mass functions significantly different from that in the solar neighborhood.

Subject headings: H II regions — infrared: interstellar: continuum — Magellanic Clouds — stars: formation

1. INTRODUCTION

Two of the many unknown facets of star formation are the dependence of the star formation rate (SFR) and initial mass function (IMF) on physical conditions such as density and temperature of the dust and gas, dust to gas ratio, metal abundance, and velocity dispersion. Another uncertainty is the influence of environmental conditions, such as the proximity of other star-forming regions. So far, no significant variations have been found in the IMF averaged over scales of a kpc, but variations have been observed on scales of open clusters. There is also indirect evidence for truncation of the IMF at the lower end in "starburst" events. For an exhaustive review of the observations, see Scalo (1986).

More determinations of the IMF in regions containing various conditions are needed to gain an understanding of how the IMF depends on local conditions. Unfortunately, a SFR or IMF is difficult to determine observationally. Mass functions are generally only directly determined by counting stars in our Galaxy, and SFRs are usually inferred from Hα or radio observations of extragalactic star-forming regions by assuming an IMF. If it were possible to indirectly but accurately infer the SFR and IMF of unresolved regions in other galaxies, it would greatly increase the sample and thus the range in physical and environmental conditions where star formation could be studied. Indirect methods are in use but are presently uncalibrated, as well as depending on many assumptions such as the nebula being ionization bounded (cf. DeGioia-Eastwood 1984). A long-range goal of this work is to find an effective, accurate method with which to determine the IMF of extragalactic, unresolved star-forming regions.

The Magellanic Clouds lie at an ideal distance for studies that can bridge the gap between resolved and unresolved regions of current star formation. The distance is such that the brighter stars can be individually observed at optical wavelengths, but most H II regions appear as only slightly extended sources at radio and infrared wavelengths. Thus the optical observations of individual stars can serve to check conclusions which would be drawn from data at longer wavelengths. In this manner the Magellanic Clouds can serve as a calibration of models designed to do extragalactic studies.

In addition to their convenient distance, the Magellanic Clouds have other attributes well suited to studies of star formation. Not only is there a wealth of observational data available, but the galaxy is forming massive stars very vigorously. There are more O3 stars identified in the LMC than have been found in our entire Galaxy, and the 30 Dor nebula is more similar to the giant H II regions we observe in external galaxies than anything we have found in our own Galaxy (Walborn 1986 and references therein).

Theoretically, it is not surprising that the LMC forms massive stars easily. For example, Wolfire & Cassinelli (1986) have carried out numerical calculations of accretion onto very massive stars, and find that in order for accretion to occur the dust must be depleted relative to Galactic conditions. Compared to the Mathis, Rumpl, & Nordsieck (1977) model, they find that the dust must be depleted relative to the gas by a factor of 4, and that large graphite grains must be depleted relative to smaller grains. It is now well accepted that the LMC has a lower metallicity and smaller dust-to-gas ratio than our Galaxy (Fitzpatrick 1985; Clayton & Martin 1985; Koornneef 1984; Dufour 1984), thus making the LMC a likely place to search for an overabundance of massive stars.

In this work we present infrared observations, obtained by the *IRAS* satellite, of H II regions in the LMC. These observations are intrinsically useful because we know the physical conditions represented: regions of recent, massive star formation, where the heating source is very likely to be stellar rather than the general interstellar radiation field (GISRF). As such the observations become building blocks for the interpretation of far-infrared emission from unresolved galaxies, which are often modeled as sums of star-forming and GISRF components (de Jong & Brink 1987; Lonsdale & Helou 1987; Rowan-Robinson 1987).

[1] This research was supported in part under NASA's *IRAS* Data Analysis Program and funded through the Jet Propulsion Laboratory.

TABLE 1

GENERAL DATA FOR THE REGION

H II REGION[a]	DEM[b]	*IRAS* POSITION[c] (1950) R.A.	Decl.	APERTURE	$S_{5\ GHz}$[d] (Jy)	Hα[e] (10^{-12} ergs) $cm^{-2}\ s^{-1}$)	Hα/Hβ[f]
MC 18	34	$04^h57^m10^s$	−66°27′17″	13′	3.37 ± 0.30	2900 ± 300	3.21
MC 47	199	05 26 46	−68 50 34	9	0.64 ± 0.06	739 ± 80	3.47
MC 57	229	05 32 36	−67 44 41	12	0.81 ± 0.10	690 ± 70	3.41
MC 64	241	05 35 51	−67 36 41	14	1.65 ± 0.06	1120 ± 100	3.84
MC 71	246[g]	05 36 23	−69 40 35	12	0.55 ± 0.06	480 ± 50	3.35
MC 90+91	323, 322, +325	05 48 44	−70 05 08	10	0.87 ± 0.11	470 ± 50	3.30

[a] Designation in McGee, Brooks, & Batchelor 1972.
[b] Designation in Davies, Elliot, & Meaburn 1976.
[c] Approximate position.
[d] Flux densities from McGee, Brooks, & Batchelor 1972.
[e] Fluxes taken from Kennicutt & Hodge 1986, as discussed in the text.
[f] Ratios taken from Caplan & Deharveng 1986.
[g] Represents only part of DEM 246.

We then combine the *IRAS* observations with existing Hα, radio, and optical data to model the stellar content of the regions. A version of the analytical H II region model first proposed by Petrosian, Silk, & Field (1972) is combined with a series of model zero-age star clusters to estimate the slope of the initial mass function in each observed region. For three of the regions, individual stellar observations are available for comparison with the models; one region in particular is used to set the normalization of the model mass function. In this work we explore the usefulness of this simple model in estimating the stellar content of our observed regions from spatially unresolved data.

2. THE DATA

The infrared data were obtained from co-added survey data taken by the *IRAS* satellite. The instrumentation, filters, and calibration are described by Neugebauer et al. (1984) and in the *IRAS* Catalogs and Atlases, Explanatory Supplement (1985). All processing was done at IPAC. The final photometry was obtained from Walter Rice's aperture photometry program, APPHOT, after the determination of the local background. Since the LMC is an extremely crowded region, the six H II regions were chosen to be relatively isolated, and the background was very carefully determined for each region. For the more crowded regions, the background level was chosen by averaging the values of many different points picked by visual inspection on the Jupiter image processing system. For the relatively isolated regions, the background was determined from the annular photometry produced by APPHOT at the radius where the flux leveled off.

Since the objective was to compare the infrared flux with that at Hα and radio wavelengths, the "aperture" was carefully chosen in each case to match those at the other wavelengths. The size was picked to correspond with the extent of the 0.1 T_b contour in the radio, which generally coincided with contours of similar shape at Hα. Note that the chosen aperture did not necessarily coincide with the entire extent of the region in the infrared; sometimes the region of infrared emission was greater than that of the Hα or radio. The 5 GHz flux densities and contour maps were taken from McGee, Brooks, & Batchelor (1972). The Hα/Hβ ratios are taken from Caplan & Deharveng (1986). The Hα fluxes were taken from the work of Kennicutt & Hodge (1986) and from their original digitized data, kindly supplied by R. Kennicutt. Table 1 contains the designations, coordinates, adopted aperture in arcminutes, radio flux densities $S_{5\ GHz}$, Hα fluxes, and Hα/Hβ ratios for the six regions.

Table 2 contains the new infrared flux densities, S_ν, as well as the 100/60 and 25/12 ratios. The flux densities in Table 2 have been corrected using the factors contained in Table VI.C.6 of the *IRAS* Supplement. The 60 and 100 μm data were corrected according to the 100/60 color temperature, the 25 μm data, according to the 60/25 color temperature, and the 12 μm data, according to the 25/12 color temperature.

Unfortunately the sizes of the regions in the infrared lie in an awkward "gray area" of a few *IRAS* beam widths. The uncertainties on photometry done with IPAC software on objects in this size regime have been found to be much greater than those for point sources or truly extended objects (W. Rice, private communication). As recommended by the IPAC staff on the basis of the software used, the uncertainties in the flux densities

TABLE 2

OBSERVED INFRARED COLOR-CORRECTED FLUX DENSITIES AND FLUX DENSITY RATIOS OF REGIONS

REGION	S_ν (Jy) 12 μm	25 μm	60 μm	100 μm	100/60	25/12
MC 18	51.8 ± 13.0	196.0 ± 49.0	1229 ± 307	2029 ± 507	1.7 ± 0.6	3.8 ± 1.3
MC 47	13.0 ± 3.3	61.5 ± 15.4	307 ± 77	363 ± 91	1.2 ± 0.4	4.7 ± 1.7
MC 57	16.1 ± 4.0	55.2 ± 13.8	337 ± 84	509 ± 127	1.5 ± 0.5	3.4 ± 1.2
MC 64	23.1 ± 5.8	107.0 ± 26.8	524 ± 131	826 ± 207	1.6 ± 0.6	4.6 ± 1.6
MC 71	22.3 ± 5.6	66.0 ± 16.5	594 ± 149	819 ± 205	1.4 ± 0.5	3.0 ± 1.0
MC 90+91	10.1 ± 2.5	30.7 ± 7.7	204 ± 51	382 ± 96	1.9 ± 0.7	3.0 ± 1.1

TABLE 3

CALCULATED PROPERTIES OF THE REGIONS

Region	T^a (K)	F_{IR} (10^{-8} ergs s^{-1} cm^{-2})	$L_{IR}/L_\odot$ ($\times 10^6$)	$E(B-V)^b$	N_{Lyc} ($\times 10^{50}$ s^{-1})
MC 18	34.7	1.28	10.7	0.07	8.2
MC 47	35.0	2.36	1.98	0.14	1.6
MC 57	35.7	3.25	2.73	0.13	2.0
MC 64	35.4	5.25	4.41	0.24	4.0
MC 71	35.6	5.28	4.43	0.11	1.3
MC 90+91	31.1	2.31	1.94	0.10	2.1

[a] Average dust temperature derived from the 60/100 ratio and an emissivity proportional to λ^{-2}.

[b] Derived from the observed Hα/Hβ ratios observed by Caplan & Deharveng 1986, corrected for a foreground reddening of 0.034.

have been conservatively adopted as 25% for each determination.

The average dust temperature and total flux in the infrared depend on the emissivity law assumed. Based on the model of interstellar grains by Draine & Lee (1984), we consider the case of emissivity proportional to λ^{-2} to be most appropriate and use this emissivity in all our calculations. In fact, however, our calculations are not very sensitive to the chosen emissivity law since in the model presented here we use only the total infrared flux, not the average temperature. The total infrared flux is relatively insensitive to changes in the emissivity law, varying less than 20% between an emissivity proportional to λ^{-2} and an emissivity proportional to λ^0.

For our total infrared fluxes we have integrated under a spline fit to the *IRAS* data points from 12 to 60 μm. We have fit a Planck function multiplied by an emissivity proportional to λ^{-2} to the 60 and 100 μm data points and have integrated under that curve from 60 to 2000 μm. The L_{IR} derived from this integration is in fact a lower limit to the true L_{IR}, since the *IRAS* bandpasses cannot detect the presence of very cold dust. The average color temperature T, integrated infrared fluxes F_{IR}, and infrared luminosity $L_{IR}/L_\odot$ are presented in Table 3. The luminosities were calculated from the fluxes using a distance for the LMC of 51.8 kpc (Welch et al. 1987).

Figure 1 is a plot of λF_λ versus λ for all six regions. The spectra for all six regions are similar. For MC 18 we have plotted a sample best-fit blackbody multiplied by an emissivity proportional to λ^{-2}. The curve is normalized to the 100 μm data point. The excess emission at 12 and 25 μm could be due to a component of very small dust grains or polycyclic aromatic hydrocarbons (PAHs; Weiland et al. 1986 and references therein), or simply emission from grains warmer than the average temperature. Further studies are in progress in the LMC (Gallagher, DeGioia-Eastwood, & Hunter 1992) to determine the nature of the LMC short-wavelength emission.

3. THE MODELS

3.1. *The* H II *Region Model*

The H II regions have been modeled using the analytic model of Petrosian et al. (1972). They originally expressed their result as

$$L_{IR} = L_{Ly\alpha} + (1-f)\langle h\nu\rangle_{Lyc} N_{Lyc} + L_{\nu<Lyc}(1-e^{-\tau'}), \quad (1)$$

where L_{IR} is the infrared luminosity of the region, f is the fraction of Lyman continuum photons absorbed by the gas, N_{Lyc} is the flux of stellar Lyman continuum photons, and τ' is an average dust absorption optical depth for wavelengths longward of the Lyman limit. $L_{Ly\alpha}$ is the luminosity of the H II region in the Lyα line, where $L_{Ly\alpha} \approx 2/3\ h\nu_\alpha N_{Lyc} f$. Equation (1) can be rewritten as

$$L_{IR} = L_{Ly\alpha} + (1-f)P_c L_{tot} + (1-e^{-\tau})(1-P_c)L_{tot}, \quad (2)$$

where L_{tot} is the total stellar luminosity and P_c is the fraction of the total stellar luminosity in the Lyman continuum.

This expression has three terms which contribute to the infrared luminosity of the region. The first expresses the absorption by dust grains of all Lyman-alpha photons produced by the gas. The second term represents direct absorption of stellar Lyman-continuum photons by the dust in competition with the gas. The third term represents direct absorption by the dust of stellar photons not in the Lyman continuum, which in practice will be in the 1000–3000 Å range. The optical depth τ' is the effective absorption optical depth of dust both in the H II

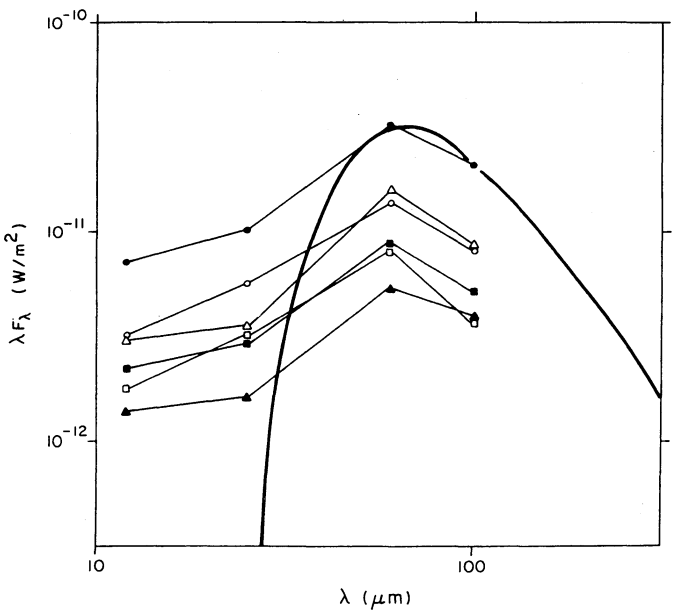

FIG. 1.—λF_λ plotted against λ for all six regions. The filled circles are for MC 18, the open triangles, for MC 71, the open circles, for MC 64, the filled squares, for MC 57, the open squares, for MC 47, and the filled triangles, for MC 90+91. The solid curve normalized to the 100 μm data point for MC 18 represents the Planck function multiplied by an emissivity proportional to λ^{-2} for $T = 35$ K, which is the best-fit average temperature for MC 18 for that emissivity.

region and in the surrounding H I region for these photons. The model of Petrosian et al. (1972) does not take scattering into account, and thus τ' is the equivalent optical depth if all the dust was gathered into a blanketing layer around the nebula.

For an H II region consisting of a single star, the third term is relatively very small and can be discarded. However, for an OB cluster, the third term contributes substantially to the infrared luminosity since the fraction of stellar flux outside the Lyman continuum is much greater than for a single OB star. The B stars are the greatest contributors, and B supergiants in an evolved OB cluster could be quite significant.

3.2. *The Model Star Clusters*

For our model star clusters we have distributed main sequence stars using a power-law mass function parameterized by the slope. Using the notation of Scalo (1986), if $f(m)$ is the number of stars born per unit mass interval dm, then $\xi(\log m) = \ln 10\, m f(m)$ equals the number of stars born per unit logarithmic mass interval, $d \log m$. In this notation,

$$\Gamma(m) = \left.\frac{\partial \xi(\log m)}{\partial \log m}\right|_m . \quad (3)$$

Thus $f(m)$ is proportional to $m^{\Gamma-1}$, and $\xi(\log m)$ is proportional to m^{Γ}.

In this notation, the original Salpeter (1955) mass function has a slope of $\Gamma = -1.3$. In his analysis of the different determinations for the mass function in the solar neighborhood, Scalo picked $\Gamma = -1.5$ as a reasonable "best" estimate for $\log m \leq 1.8$, with a value of Γ anywhere between -1.5 and -2.0 for the extrapolation to larger masses.

We have normalized our mass function such that there is one star between 65 and 76 $M_\odot$, with an upper mass limit of 70 $M_\odot$ for purposes of integration. This normalization was chosen so that our models would successfully predict the observed Γ for MC 90+91, as discussed below. Thus the region MC 90+91 serves as the calibration for the models. The lower mass limit for the model clusters was set to 0.1 $M_\odot$. One expects the calculations to be insensitive to the lower mass limit; Ho & Haschick (1981) found that the fraction of the total luminosity in the Lyman continuum is virtually independent of the lower mass limit of a cluster.

In our calculations, the mass of individual stars as a function of stellar effective temperature was derived from the observations collected in Popper (1980) and the calculations of Stothers & Chin (1977). The total luminosity for each star was taken from the average mass-luminosity relation. For stars less than 50 $M_\odot$ we used $(L_{\rm star}/L_\odot) = (M/M_\odot)^{3.3}$; for stars greater than 50 $M_\odot$ we used the main-sequence band mass–luminosity relation given by Maeder (1983) for high-mass stars. The number of Lyman-continuum photons and bolometric correction as a function of effective temperature were derived from Pangia (1973).

The calculated properties of each model cluster include the total luminosity of the cluster ($L_{\rm tot}$), the fraction of the total luminosity in the Lyman continuum (P_c), the total mass of the cluster in solar masses ($M_{\rm tot}$), the integrated absolute V magnitude (M_V), and the bolometric correction of the integrated light (BC). Each of these quantities was calculated as a function of Γ, the slope of the mass function. The properties of these model clusters are presented in Table 4.

Models using $\Gamma = -1.5$ below 12 $M_\odot$ and $\Gamma = -1.8$ above 12 $M_\odot$, which approximates Scalo's (1986) best guess for the solar neighborhood, give results virtually indistinguishable from $\Gamma = -1.8$. This confirms that it is only the most massive stars which matter for these calculations.

For additional flexibility in our models, we included the capability of multiplying the total number of stars by two or more. In effect, this changes the normalization such that there are two or more of the most massive stars present. This new normalization changes the total luminosity and total mass of the cluster, but leaves the fraction of the total luminosity in the Lyman continuum unchanged. As we shall see later, the integrated V magnitude of the cluster serves as an observational quantity which could distinguish between normalizations. However, since no supergiants have been included in the model clusters, these V magnitudes serve as lower bounds.

4. FITTING THE OBSERVATIONS TO THE MODELS

4.1. *The Observed Luminosities*

The first term in equation (2), $L_{\rm IR}$, has been fitted by our new observations of the infrared luminosity, which has already been discussed and presented in Table 3. The next term, $L_{\rm Ly\alpha}$, is fitted from the 5 GHz observations by McGee et al. 1972) discussed earlier. As noted earlier, $L_{\rm Ly\alpha} = 2/3\ h\nu_{\rm Ly\alpha} N_{\rm Lyc} f$, where $N_{\rm Lyc}$ is the number of stellar continuum photons produced. Thus we can use the radio thermal emission to calculate $L_{\rm Ly\alpha}/f$.

Our rederivations of the flux of Lyman-continuum photons and $L_{\rm Ly\alpha}$ expected from the observed radio thermal emission are $N_{\rm Lyc} = S_\nu D^2$ (9.08×10^{46}) and thus $L_{\rm Ly\alpha}/f = S_\nu D^2$ (9.90×10^{35}), where D is the distance in kpc, $L_{\rm Ly\alpha}$ is the luminosity in ergs s^{-1}, and S_ν is the 5 GHz flux density in Jy. We have assumed $T = 10^4$ K, $Z = 1$, and $g_{\rm ff} = 5.06$. The derived values of $N_{\rm Lyc}$ are presented in Table. 3.

One observational uncertainty with the application of this model stems from the assumption that all the radio flux measured at 5 GHz is due to thermal emission; in reality it is possible that the 5 GHz flux is contaminated by nonthermal emission as well. However, contamination by nonthermal emission is more of a problem for global observations of galaxies than for individual H II regions, and in irregular galaxies is not a significant effect even for global measurements (Klein 1988). In the LMC in particular, the mean spectral index of the entire galaxy is significantly flatter than that of a normal spiral (Klein et al. 1989). The fraction of thermal radiation at 2.3 GHz, averaged over the entire galaxy is 65% ± 20% (Klein et al. 1989).

For each of the regions considered here we have examined the radio spectral indices given by McGee & Newton (1972). Four of the six are flat, i.e., $\alpha \geq -0.2$, and can be considered entirely thermal. Two of the six have $\alpha \approx -0.46$ and thus are contaminated by nonthermal emission. We have numerically experimented with the effects of nonthermal emission by running the same models with radio flux densities about 65% of the nominal value, representing an average fraction of thermal emission. The effects are such that if nonthermal contamination is suspected for a given region, then the true mass function will be slightly steeper than the one determined by the models. The size of the effect is only a change of about 0.1 in the slope of the mass function. The effects of this contamination on the conclusions for specific regions are discussed in § 5.

TABLE 4

PROPERTIES OF THE MODEL STAR CLUSTERS

Γ	L_{tot} ($L_\odot$)	P_c	M_{tot} ($M_\odot$)	M_V (mag)	BC (mag)
−0.1	0.2294E+07	0.560	0.5414E+03	−6.91	−4.29
−0.2	0.2376E+07	0.556	0.6074E+03	−6.96	−4.28
−0.3	0.2464E+07	0.552	0.6905E+03	−7.01	−4.27
−0.4	0.2558E+07	0.548	0.7977E+03	−7.07	−4.25
−0.5	0.2658E+07	0.544	0.9392E+03	−7.12	−4.24
−0.6	0.2767E+07	0.539	0.1131E+04	−7.18	−4.23
−0.7	0.2883E+07	0.534	0.1398E+04	−7.24	−4.21
−0.8	0.3010E+07	0.529	0.1780E+04	−7.30	−4.20
−0.9	0.3147E+07	0.523	0.2342E+04	−7.36	−4.18
−1.0	0.3296E+07	0.517	0.3191E+04	−7.43	−4.17
−1.1	0.3459E+07	0.510	0.4505E+04	−7.50	−4.15
−1.2	0.3638E+07	0.503	0.6587E+04	−7.58	−4.13
−1.3	0.3835E+07	0.495	0.9951E+04	−7.66	−4.10
−1.4	0.4053E+07	0.486	0.1549E+05	−7.74	−4.08
−1.5	0.4296E+07	0.477	0.2474E+05	−7.83	−4.05
−1.6	0.4567E+07	0.466	0.4043E+05	−7.93	−4.02
−1.7	0.4873E+07	0.455	0.6732E+05	−8.03	−3.99
−1.8	0.5220E+07	0.443	0.1139E+06	−8.14	−3.95
−1.9	0.5617E+07	0.429	0.1954E+06	−8.26	−3.91
−2.0	0.6075E+07	0.414	0.3388E+06	−8.40	−3.86
−2.1	0.6609E+07	0.398	0.5930E+06	−8.54	−3.81
−2.2	0.7240E+07	0.380	0.1046E+07	−8.71	−3.74
−2.3	0.7995E+07	0.361	0.1859E+07	−8.89	−3.67
−2.4	0.8912E+07	0.340	0.3321E+07	−9.10	−3.58
−2.5	0.1005E+08	0.317	0.5964E+07	−9.33	−3.48
−2.6	0.1148E+08	0.291	0.1076E+08	−9.59	−3.36
−2.7	0.1332E+08	0.264	0.1948E+08	−9.88	−3.23
−2.8	0.1576E+08	0.236	0.3540E+08	−10.21	−3.08
−2.9	0.1907E+08	0.206	0.6452E+08	−10.58	−2.92
−3.0	0.2368E+08	0.175	0.1179E+09	−10.99	−2.75
−3.1	0.3027E+08	0.145	0.2161E+09	−11.42	−2.58
−3.2	0.3997E+08	0.116	0.3968E+09	−11.90	−2.41
−3.3	0.5462E+08	0.090	0.7302E+09	−12.40	−2.25
−3.4	0.7729E+08	0.068	0.1346E+10	−12.92	−2.10
−3.5	0.1132E+09	0.049	0.2486E+10	−13.47	−1.97
−3.6	0.1712E+09	0.035	0.4599E+10	−14.03	−1.85
−3.7	0.2667E+09	0.024	0.8518E+10	−14.61	−1.75
−3.8	0.4262E+09	0.016	0.1580E+11	−15.21	−1.67
−3.9	0.6964E+09	0.010	0.2935E+11	−15.81	−1.60
−4.0	0.1160E+10	0.007	0.5457E+11	−16.42	−1.54

4.2. *The Observed Optical Depth and f*

For each region we have estimated the "observed" value of τ' by extrapolating from observed values for the extinction in the visible regime into the ultraviolet. We started with the Hα/Hβ ratios observed by Caplan & Deharveng (1986), listed in Table 1, and converted these ratios to color excesses, $E(B-V)$, by interpolation in Table 2 of Savage & Mathis (1979). It is legitimate to use this standard Galactic optical extinction curve since Fitzpatrick (1985) showed that interstellar reddening in the LMC is virtually indistinguishable from that of our Galaxy in the optical regime. Using Hα/Hβ ratios to estimate the extinction is also legitimate since A_V is less than 1 mag for all six regions considered here, and less than half a magnitude for all but two of the regions. At these relatively low extinctions the Hα/Hβ ratio is a good indicator of the true optical depth whether the dust is in a blanketing layer or mixed in with the gas (Mathis 1970). In MC 90+91, the one region where we have $E(B-V)$ derived from both stellar UBV photometry and the Balmer decrement, the two agree very well (see § 4). The foreground reddening was taken to be $E(B-V)=0.034$ (McNamara & Feltz 1980). The adopted values of $E(B-V)$ for each region, already corrected for foreground reddening, are included in Table 3.

Fitzpatrick (1985) showed that the differences between LMC and Galactic reddening are substantial in the ultraviolet, so his derivation of the non–30 Dor LMC ultraviolet extinction curve was then used to extrapolate $E(B-V)$ down to the ultraviolet. We derived an average A_{UV} in the 0.1–0.3 μm region by weighting his tabulated values of $A_{UV}/E(B-V)$ over the UV continuum of a 60 $M_\odot$ star. The use of a 60 $M_\odot$ star was reasonable since Massa & Savage (1985) determined for the UV continua of all O stars are very similar; the fluxes we used were taken from their work. Our weighted average value for $A_{UV}/E(B-V)$ was 9.6. After thus calculating the average ultraviolet extinction A_{UV}, we then calculated the average absorption optical depth τ' using the relationships

$$\tau = \frac{\tau'}{1-\omega} = \frac{A_{UV}}{1.086}, \tag{4}$$

where τ represents the total optical depth, τ' represents the absorption optical depth only, and ω is the albedo. From the work of Draine & Lee (1984), we have taken the albedo to be

TABLE 5

MODELED PROPERTIES OF THE REGIONS

Region	τ'	f	Γ
MC 18	0.32 ± 0.11	0.79 ± 0.07	-1.8[a]
MC 47	0.63 ± 0.16	0.62 ± 0.08	-1.5 ± 0.6
MC 57	0.56 ± 0.15	0.65 ± 0.08	-2.1 ± 0.4
MC 64	1.04 ± 0.25	0.45 ± 0.09	-2.1 ± 0.4
MC 71	0.49 ± 0.14	0.69 ± 0.08	-1.9[a]
MC 90+91	0.43 ± 0.13	0.72 ± 0.08	-1.7 ± 0.5

[a] Using a different normalization; see text.

0.5. The value for τ' calculated for each region is presented in Table 5.

The uncertainty in each calculated τ' was estimated as follows. The precision of Caplan & Deharveng's (1986) photometry was about 1%, so the uncertainty in $E(B-V)$ was taken to be 0.01 mag. The uncertainty in the foreground extinction was taken as 0.01 in $E(B-V)$ (McNamara & Feltz 1980). The uncertainty in converting $E(B-V)$ to a weighted ultraviolet τ from Fitzpatrick's data was estimated at 10%, and the value of the dust albedo was taken to be 0.5 ± 0.1. Thus the total 1 σ uncertainty for the calculated values of the absorption-only ultraviolet τ' ranged from $\pm 21\%$ to $\pm 36\%$.

One of the results of the analytic H II region model by Petrosian et al. (1972) used in this work is an analytic expression for f, the fraction of Lyman-continuum photons absorbed by the gas in competition with the dust, as a function of the optical depth. The expression they give is

$$f = \frac{\frac{1}{3}\tau'^3 \exp(-\tau')}{\tau'^2 - 2\tau' + 2[1 - \exp(-\tau')]}, \quad (5)$$

where τ' is the same absorption-only, average UV τ' used in equations (1) and (2). The value of f calculated for each region, and its uncertainty resulting from the uncertainty in τ', is included in Table 5. Note that f is not a strong function of τ', and that the values of f for all the regions are similar.

4.3. *Determining the IMF*

The models and observations described above are used to determine the IMF of a region as follows. For each region, equation (2) is solved for the expected optical depth, τ', using the observed luminosities L_{IR} and $L_{Ly\alpha}$ and model star cluster properties P_c and L_{tot} as a function of Γ, the slope of the mass function of the model cluster. The expected optical depth as a function of Γ is then compared to the observed optical depth to determine Γ. Note that when calculating the expected absorption optical depth, τ', as a function of Γ it is also necessary to specify f; the value of f used for each region was calculated from the observed optical depth using equation (5). The values for the observed optical depth and f used for each region are summarized in Table 5.

As an example, Figure 2 shows the expected τ' from equation (2) as a function of Γ, the slope of the IMF in the model star cluster used to produce P_c and L_{tot}, for the region MC 90+91. The calculations were made with an f of 0.72. The observed value of τ' is 0.43, which intersects the curve at $\Gamma = -1.7$. Thus our predicted value of the slope of the mass function for MC 90+91 is -1.7. As discussed below in § 5, the mass function has been directly determined for the OB associations Lucke-Hodge 117 and 118 inside MC 90+91, and the normalization for our model star clusters was chosen to reproduce that slope.

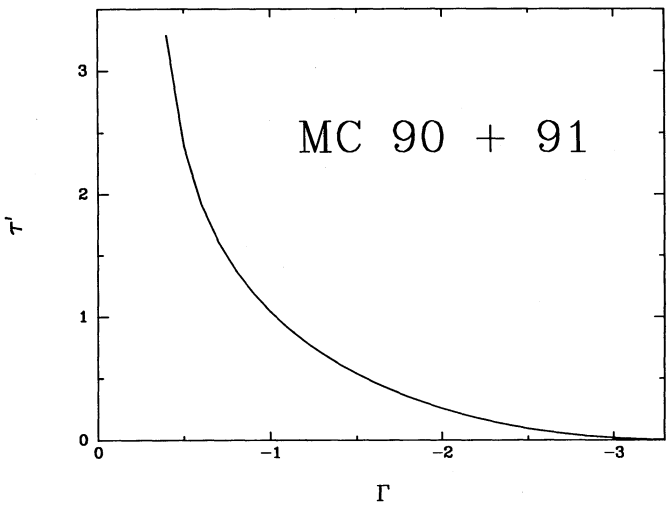

FIG. 2.—The solution to eq. (2) for the region MC 90+91, as described in the text. Γ is the slope of the initial mass function for the model star cluster producing L_{tot} and P_c, and τ' is the resulting absorption-only UV optical depth for the observed L_{IR} and $L_{Ly\alpha}$. The fraction f has been set to 0.72.

The primary uncertainties in the determination of Γ are the large uncertainty in τ' and the 25% uncertainties in L_{IR}. The uncertainty in Γ resulting from the uncertainty in τ' can be read directly off Figure 2 and translates to an uncertainty of about 0.2 in Γ for an uncertainty of 0.13 in the value of τ' for MC 90+91. This value of 0.2 is typical for all six regions presented here. Estimating the uncertainty in Γ from the uncertainty in L_{IR} is less straightforward. We have rerun the models for MC 90+91 using 125% of L_{IR} and 75% of L_{IR}; the difference in the resulting values for Γ is about ± 0.5. This value is also typical for all the regions. Since the two uncertainties in Γ are independent, the total resulting uncertainty is the RMS sum of the two, or about 0.54.

The estimated model value for Γ for each region and its uncertainty are discussed in the next section. A summary of the values is provided in Table 5.

It is worthwhile to examine the values plotted in Figure 2 to find the relative importance of the various terms in equation (2). There are no solutions to equation (2) for a cluster with Γ as small as -0.1. For low values of Γ, say ≈ -0.5, there will be solutions but L_{tot} is low compared to higher values of Γ. Even though P_c is fairly high, the first and second terms are not enough to produce the observed L_{IR}, and τ' must be high in order for the third term to produce enough luminosity. Thus in order to produce the observed L_{IR}, a cluster with such a flat IMF would have to be very dusty to make up for its intrinsic lack of luminosity.

In the regime of high values of Γ, say ≈ -3.0, the second term in equation (2) dominates: even though P_c is small, L_{tot} has become very large, and the second term produces almost all the needed infrared luminosity. Thus τ' has to be very small to keep the third term from contributing very much. This corresponds to no dust surrounding the H II region. However, since with this model f is held constant and non-zero, there must be internal dust. This case would be geometry-dependent, and thus our model is not reliable in this regime. However, all our observed regions fall in the middle regime between the extremes, where all three terms are contributing, and should be trustworthy.

5. ANALYSIS OF INDIVIDUAL REGIONS

5.1. *MC 90+91*

First we consider the region MC 90+91 (DEM 323+322+325), which lies about 1°.5 (1.3 kpc) southeast of 30 Dor. This region serves as the calibrator for the normalization of the cluster models for two reasons: (1) detailed photometric and spectroscopic observations of the stars in both the OB associations are available (Massey et al. 1989), and (2) the 5 GHz emission is entirely thermal. There are two other regions in our sample for which the mass function has been directly determined, but either the radio emission was not entirely thermal, or there were several OB associations contained within the region and not all of them had been studied.

Massey et al. (1989) determined the slope of the high-mass end of the current mass function for the region. Using the notation discussed in § 3, they found a value for Γ of -1.8 for LH 117 and LH 118 combined, with a formal error of 0.1. As discussed earlier, this is within the range of estimates for massive stars in the solar neighborhood. The earliest spectral type observed was O3–O4. In their mass function the highest bin was 60–90 $M_\odot$, in which there was one star. There were two stars in their second bin, 40–60 $M_\odot$.

Massey et al. also found that the extinction derived from two-color photometry (without the foreground reddening removed) for the association stars is variable from star to star, with the most probable $E(B-V)$ equal to 0.12 for the OB association Lucke-Hodge 117, and a value of 0.10 for Lucke-Hodge 118, both associated with the region. Our value for $E(B-V)$ of 0.13 derived from the Hα/Hβ ratios of Caplan & Deharveng (1980) is in good agreement with these measurements. McGee & Newton (1972) give a radio spectral index of $\alpha = -0.19$ for MC 91, the brighter of the two regions in the radio, and a spectral index of $\alpha = -0.28$ for MC 90. Thus the radio emission can be considered to be entirely thermal.

As discussed earlier, the normalization of the mass function in our model star clusters was chosen to produce a predicted Γ of -1.7 ± 0.5, which is in agreement with the value of -1.8 ± 0.1 found by Massey et al. The uncertainty in the predicted Γ includes the uncertainties in τ' and in $L_{\rm IR}$.

5.2. *MC 47*

The region MC 47 (DEM 199) is well separated from the 30 Dor complex, lying $\sim 1°$ (900 pc) distant to the northwest. J. Parker and C. Garmany (private communication) have obtained preliminary results for the mass function for this region of $\Gamma = -2.0 \pm 0.2$. Inspection of Figure 3 shows that for our observed τ' of 0.63, we predict a Γ of -1.4.

The uncertainty introduced in Γ by the uncertainty in τ' is about 0.2, while the uncertainty in $L_{\rm IR}$ produces an additional uncertainty of 0.55. The two independent uncertainties together make an uncertainty of 0.6. In addition, the value for the radio spectral index for this region given by McGee & Newton (1972) is $\alpha = -0.46$, indicating some contamination by nonthermal emission. Thus our models would indicate a slope slightly steeper than the nominal best-fit value; running the models with $L_{\rm Ly\alpha}$ set at 65% of the observed value gives a Γ steeper by about 0.1 (a systematic error). Thus our best estimate for the model value is $\Gamma = -1.5 \pm 0.6$, which agrees with the observed value within the uncertainties.

5.3. *MC 18*

The radio source MC 18 (DEM 34) is the large, relatively isolated H II region at the far northwest corner of the LMC.

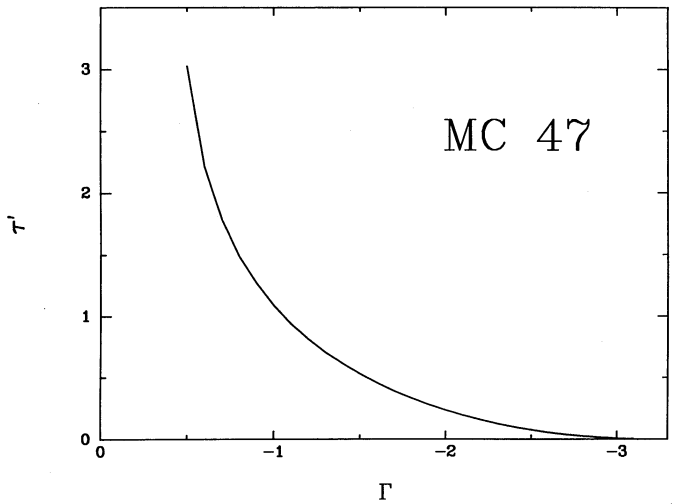

FIG. 3.—Same as Fig. 2 for the region MC 47; the fraction f has been set to 0.62.

Comparing a CO map (Cohen et al. 1988), an H I map (McGee & Milton 1966), and an overall FIR map (Rice et al. 1988), strong Hα and FIR emission appear at two ends of a large gas complex seen in H I and CO. Thus MC 18 appears to be at one end of a double H II blister. The entire complex contains the OB associations LH 9, 10, 13, and 14. Even though there is a possible supernova remnant associated with the region, the overall radio spectral index is $\alpha = +0.01$, indicative of predominantly thermal emission.

Parker & Massey (1992) have photometric and spectroscopic observations for the stars in LH 9 and 10. Their preliminary results indicate that the reddening is higher for LH 10 than for LH 9, and they find a flatter mass function, $\Gamma = -1.0$, for LH 10. They find that LH 9 has a "normal" mass function, $\Gamma = -1.7$. However, these represent only a fraction of the stars in MC 18, and thus it is impossible to compare these results to our models directly.

In Figure 4 we show the run of Γ versus τ' for MC 18, with f set equal to 0.79. Keeping the mass function normalized to one

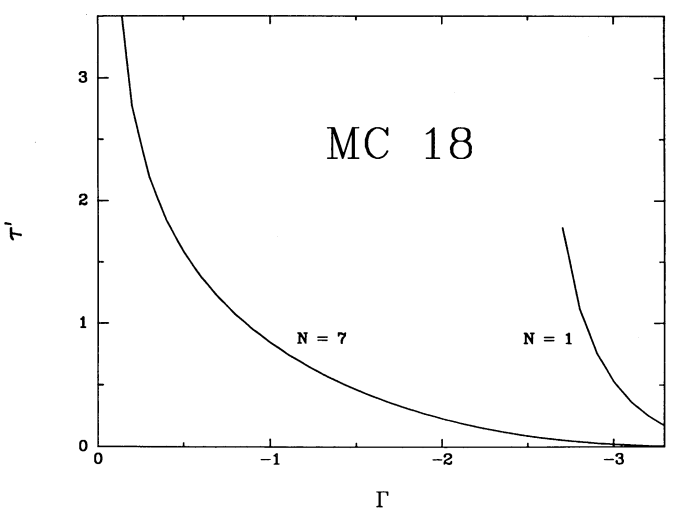

FIG. 4.—Same as Fig. 2 for the region MC 18; the fraction f has been set to 0.79. The curve labeled $N = 1$ corresponds to the normalization of the mass function in the model star cluster such that there is one star between 65 and 75 $M_\odot$ present; the curve labeled $N = 7$ corresponds to seven stars in that same interval.

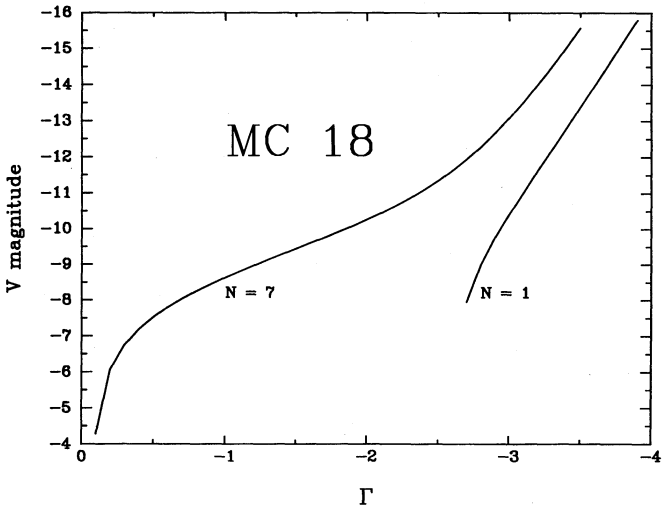

FIG. 5.—The calculated integrated absolute V magnitude of the model star clusters used for MC 18 as a function of the slope of the initial mass function of the cluster, Γ. At each Γ the magnitude has been reddened appropriately according to Fig. 4. The curve labeled $N = 1$ corresponds to the normalization of the mass function in the model star cluster such that there is one star between 65 and 75 $M_\odot$ present; the curve labeled $N = 7$ corresponds to seven stars in that same interval. These magnitudes represent lower limits since no supergiants have been included.

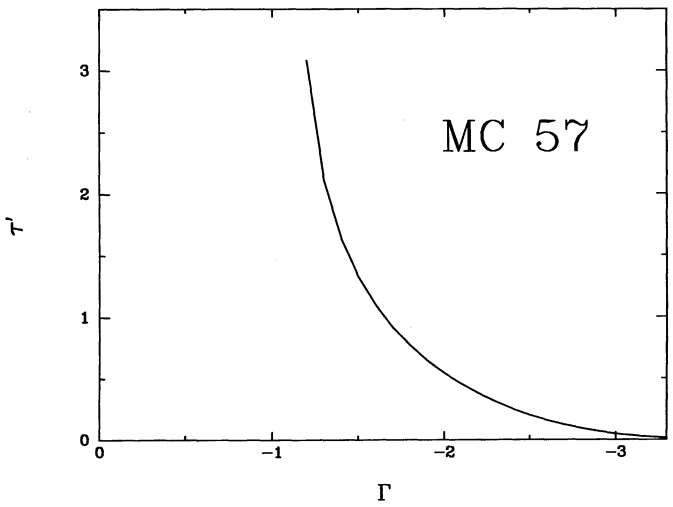

FIG. 6.—The same as Fig. 2 for the region MC 57; the fraction f has been set to 0.65.

star at the top, the slope for the mass function derived from our data for MC 18 is $\Gamma = -3.1$. However, a solar neighborhood function, with $\Gamma = -1.8$, can be obtained if the mass function is normalized so that there are seven of the most massive stars present. Since the simplest case is that of the "normal mass function and more stars, we would consider that case more likely without any additional information. In Figure 4 the curve labeled $N = 1$ corresponds to the usual normalization, while the curve labeled $N = 7$ corresponds to the normalization with seven of the most massive stars present.

However, there is an additional parameter which could help to distinguish between the two cases if the observations were available. Figure 5 shows a plot of the lower-limit integrated V magnitude as a function of Γ calculated for the model clusters as discussed in § 3 and reddened in accordance with the extinction appropriate to τ' calculated for each Γ for MC 18 as shown in Figure 2. The different loci represent the different normalizations for the mass function, where N is the number of the most massive stars present. Thus if one had the integrated V magnitude available in addition to the optical depth, one would be able to distinguish between the cases discussed above.

5.4. *MC 57 and MC 64*

The radio source MC 57 (DEM 229) lies close to MC 64 (DEM 241); both are ~0°.5 north (1.3 kpc) of 30 Dor. They are both part of the ring of H II regions surrounding Constellation III (Nail & Shapley 1953), a major OB stellar complex with very little gas or dust remaining. Neither region has direct stellar observations yet available. The plots of Γ versus τ' used to determine Γ are shown in Figures 6 and 7, with the value of f set to 0.65 and 0.45, respectively. Both regions are within the range of what can be considered a solar neighborhood mass function, with $\Gamma = -2.0 \pm 0.4$ for MC 57 and $\Gamma = -2.1 \pm 0.4$ for MC 64.

According to the observations of McGee & Newton (1972), MC 64 has a flat, thermal, radio spectrum ($\alpha = +0.08$), but MC 57 is contaminated by nonthermal emission ($\alpha = -0.46$). Our prediction for the mass function slope for MC 57 should therefore be steeper by about 0.1, or $\Gamma = -2.1 \pm 0.4$. Thus there is no evidence for a mass function any different than that in the solar neighborhood for either of these regions.

5.5. *MC 71*

The radio source MC 71 coincides with the infrared source discussed here, but the region is only part of the larger H II complex designated as DEM 246. The region is ~0°.75 (or roughly 700 pc) southwest of 30 Dor, putting it on the edge of the greater 30 Dor complex. The overall radio spectral index is $\alpha = +0.02$, indicative of primarily thermal emission. Figure 8 shows Γ versus τ' for this region, with f set equal to 0.69. The

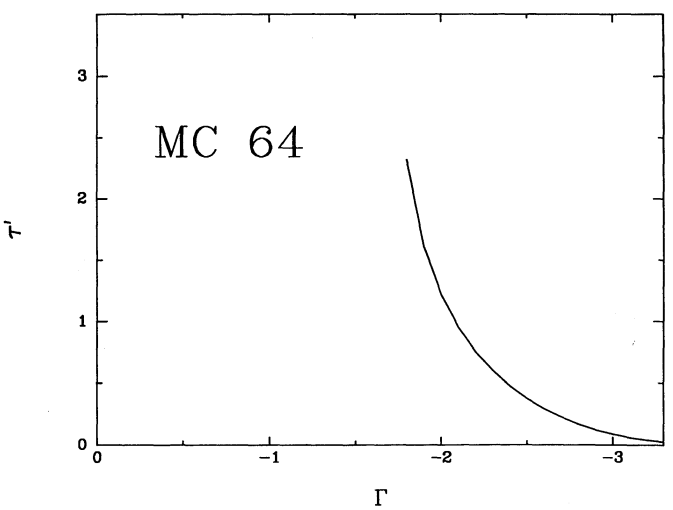

FIG. 7.—The same as Fig. 2 for the region MC 64; the fraction f has been set to 0.45.

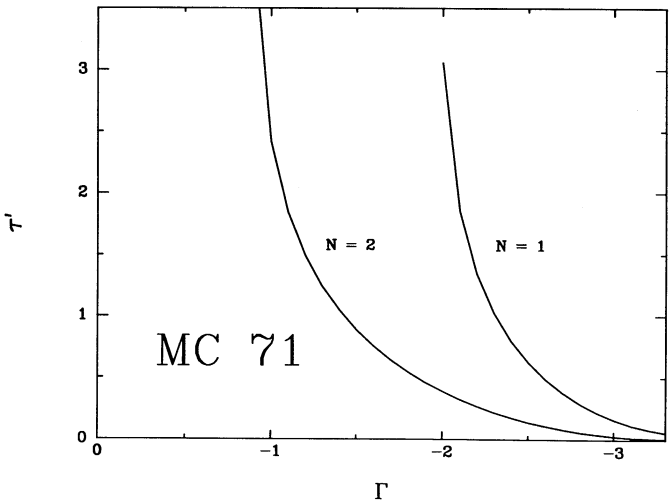

FIG. 8.—The same as Fig. 2 for the region MC 71; the fraction f has been set to 0.69. The curve labeled $N = 1$ corresponds to the normalization of the mass function in the model star cluster such that there is one star between 65 and 75 $M_\odot$ present; the curve labeled $N = 2$ corresponds to two stars in that same interval.

different loci represent different normalizations with N equal to the number of the most massive stars present. This region is nominally best fitted with a Γ of -2.6. However, a mass function normalized such that there are two of the most massive stars present with a Γ of -1.9 fits equally well. Without observations of the integrated V magnitude, this method is unable to distinguish between the two situations; thus, since the solar neighborhood fit with twice as many stars is the simpler hypothesis, as for MC 18 we assume that the simpler hypothesis is true and that there is no evidence for a mass function different from that in the solar neighborhood.

6. DISCUSSION

The models presented here do not present convincing evidence for mass functions significantly different than that in the solar neighborhood. This is contrary to the conclusions of Jones et al. (1986), who found evidence for mass functions flatter than a Miller & Scalo (1979) IMF for the H II regions MC 64, MC 75, MC 76W, and MC 77 from far-infrared observations. For each of these regions, they set the total luminosity equal to the total FIR luminosity and compared that to the number of ionizing photons derived from the thermal radio flux. They find each region to be underluminous for the amount of ionizing radiation it produces if a Miller-Scalo IMF is assumed, and if all the stellar luminosity is absorbed by the dust and reradiated in the infrared. The authors interpret this as the regions containing an excess of early O stars relative to late-O and early-B stars relative to a Miller-Scalo IMF. Since they constrain $L_{\rm tot}$ to be equal to $L_{\rm IR}$, they then interpret this as a truncation of the mass function at the low-mass end rather than a flattening. Other evidence for the truncation is the apparent absence of protostars less than about 15 $M_\odot$.

The analysis of Jones et al. rests on the assumption that $L_{\rm tot} \approx L_{\rm IR}$. They consider this a good assumption for MC 77 (N159) and MC 76W (N160A), but less convincing for the others, which are less dusty. In comparison with the regions presented here, Jones et al. have assumed $A_V > 2$ over most of MC 77, and individual sources in MC 76W were found to have even higher visual extinctions. (They did not have sufficient data to estimate A_V for the region we have in common, MC 64.) Our regions, however, all have $A_V \leq 1$. This implies that in our regions the total luminosity is not completely converted to infrared radiation, and thus $L_{\rm IR}$ is a lower limit to $L_{\rm tot}$ rather than equal to $L_{\rm tot}$. In light of this, we cannot possibly distinguish here between an IMF which is flatter and one which is truncated.

In summary, we have obtained far-infrared fluxes for six H II regions in the LMC using *IRAS* observations. The infrared spectra for the six regions are all quite similar. These regions are almost certainly heated by stellar radiation from the cluster rather than from the general interstellar radiation field, and as thus their properties can serve as building blocks for models interpreting the far infrared fluxes of unresolved galaxies.

With the long range goal of determining the stellar content of unresolved star-forming regions, we have modeled these regions in terms of a cluster of zero-age stars, using observations of the infrared and thermal luminosities and the average optical depth in the visible. In the two cases where the stars in the OB association had been studied, the model successfully predicts the slope of the observed upper mass function within the uncertainties. This simple model appears to work reasonably well and could be tightened up further by observing additional parameters. Thus this method provides hope, if the targets are chosen carefully, of determining the stellar content of unresolved extragalactic star-forming regions. The uncertainties are such that the stellar content of a single region may not be determined precisely, but in a statistical sense with a large sample the stellar content as a function of other properties might be determined.

None of these ordinary star-forming regions are found to have mass functions significantly different than that in the solar neighborhood, even though the average metallicity of the LMC is significantly lower than in our Galaxy, and even though on the average the LMC is forming stars at a rate much higher than our Galaxy. This result may not apply to extraordinary "starburst" regions such as 30 Dor, but in that case it cannot be purely a metallicity effect. This result generally validates the use of the observed infrared properties of the regions as building blocks for models of unresolved galaxies, since the mass function does not seem to be wildly variable.

The author gratefully acknowledges the contribution of J. Cassinelli, who participated in the early stages of this work, as well as useful discussions with J. Gallagher, D. Hunter, and G. Clayton. An anonymous referee also improved the paper significantly. The entire staff of IPAC, particularly W. Rice, were tremendously helpful. This work was supported by NASA under the *IRAS* General Investigator Program and through an American Astronomical Society Small Research Grant, also funded by NASA.

REFERENCES

Caplan, J., & Deharveng, L. 1986, A&A, 155, 297
Clayton, G. C., & Martin, P. 1985, ApJ, 288, 558
Cohen, R., Dane, T., Garay, G., Montani, T., Rubio, M., & Thaddeus, P. 1988, ApJ, 331, L95

Davies, R. D., Elliott, K. H., & Meaburn, J. 1976, MmRAS, 81, 89
DeGioia-Eastwood, K. 1984, PASP, 96, 625
de Jong, T., & Brink, K. 1987, in Star Formation in Galaxies (CP-2466), ed. C. J. Lonsdale-Persson (Washington, DC: NASA), 323
Draine, B. T., & Lee, H. M. 1984, ApJ, 285, 89
Dufour, R. 1984, in IAU Symp. 108, Structure and Evolution of the Magellanic Clouds, ed. S. van den Bergh & K. S. de Boer (Dordrecht: Reidel), 353
Fitzpatrick, E. L. 1985, ApJ, 299, 219
Gallagher, J., DeGioin-Eastwood, K., & Hunter, D. 1992, in preparation
Ho, P. T. P., & Haschick, A. O. 1981, ApJ, 248, 622
IRAS Catalogs and Atlases, Explanatory Supplement, 1985, ed. C. A. Beichman, G. Neugebauer, H. J. Habing, P. E. Clegg, & T. J. Chester (Washington DC.: U. S. Government Printing Office) (IRAS Supplement)
Jones, T. J., Hyland, A. R., Straw, S., Harvey, P. M., Wilking, B. A., Joy, M., Gatley, I., & Thomas, J. A. 1986, MNRAS, 219, 603
Kennicutt, R. C., & Hodge, P. W. 1986, ApJ, 306, 130
Klein, U. 1988, Ph.D. thesis, Radioastronomisches Institut der Universität Bonn
Klein, U., Wielebinski, R., Haynes, R. F., & Malin, D. F. 1989, A&A, 211, 280
Koornneef, J. 1984, in IAU Symp. 108, Structure and Evolution of the Magellanic Clouds, ed. S. van den Bergh & K. S. de Boer (Dordrecht: Reidel), 333
Lonsdale, C., & Helou, G. 1987, ApJ, 314, 513
Maeder, A. 1983, A&A, 120, 113
Massa, D., & Savage, B. D. 1985, ApJ, 299, 905
Massey, P., Garmany, C., Silkey, M., & DeGioia-Eastwood, K. 1989, AJ, 97, 107
Mathis, J. S. 1970, ApJ, 159, 263
Mathis, J. S., Rumpl, W., & Nordsieck, K. H. 1977, ApJ, 217, 425
McGee, R. X., Brooks, J. W., & Batchelor, R. A. 1972, Australian J. Phys., 25, 581
McGee, R. X., & Milton, J. 1966, Australian J. Phys., 19, 343
McGee, R. X., & Newton, L. M. 1972, Australian J. Phys., 25, 619
McNamara, D. H., & Feltz, K. A. 1980, PASP, 92, 587
Miller, G. E., & Scalo, J. M. 1979, ApJS, 41, 513
Nail, V., & Shapley, H. 1953, Proc. Natl. Acad. Sci., 39, 358
Neugebauer, G., et al. 1984, ApJ, 278, L1
Panagia, N. 1973, AJ, 78, 929
Parker, J., & Massey, P. 1992, in preparation
Petrosian, V., Silk, J., & Field, G. B. 1972, ApJ, 177, L69
Popper, D. M. 1980, ARA&A, 18, 115
Rice, W., Lonsdale, C. J., Soifer, B. T., Neugebauer, G., Kopan, E. L., Lloyd, L. A., DeJong, T., & Habing, H. J. 1988, ApJS, 68, 91
Rowan-Robinson, M. 1987, in Star Formation in Galaxies (NASA CP-2466), ed. C. J. Lonsdale-Persson (Washington, DC: NASA), 133
Salpeter, E. E. 1955, ApJ, 121, 161
Savage, B. D., & Mathis, J. S. 1979, ARA&A, 17, 73
Scalo, J. 1986, Fund. Cosmic Phys., 11, 1
Stothers, R., & Chin, C. 1977, ApJ, 211, 189
Walborn, N. 1986, in IAU Symp. 116, Luminous Stars and Associations in Galaxies, ed. C. W. H. deLoore, A. J. Willis, & P. Laskarides (Dordrecht: Reidel), 185
Weiland, J. L., Blitz, L., Dwek, E., Hauser, M. G., Magnani, L., & Rickard, L. J. 1986, ApJ, 306, L101
Welch, D. L., McLaren, R. A., Madore, B. F., & McAlary, C. W. 1987, ApJ, 321, 162
Wolfire, M. G., & Cassinelli, J. P. 1986, ApJ, 310, 207